Fibers and Polymers (2024) 25:631–649
https://doi.org/10.1007/s12221-023-00396-1

Online ISSN 1875-0052
Print ISSN 1229-9197

REGULAR ARTICLE

Anti-ultraviolet Properties of Weft-Knitted Textile Composite Materials Based on Modified Aramid and UHMWPE Fabrics

Cuiyu Li[1,2] · Jingting Shan[1] · Yueyan Cui[3] · Mengxiao Shi[1] · Changhong Feng[1] · Lei Zhang[1]

Received: 12 July 2023 / Revised: 20 September 2023 / Accepted: 5 October 2023 / Published online: 19 December 2023

Abstract

The amide bonds of aramid fibers' prolonged exposure to sunlight leads to the aging of the fibers and poor UV resistance. However, in most of the current studies, the improvement of UV resistance is accompanied by damage to aramid fibers. Four different mass fractions of the silane coupling agent KH550 and anhydrous calcium chloride were used to modify the surface of aramid fibers followed by grafting of zinc oxide nanoparticles onto the aramid fibers. The results showed that the surface free energy increased by 43.61%, and the interfacial shear strength (IFSS) increased by 58.19% when the concentration of KH550 was 20%. The tensile, flexural, and compressive strengths of the composites were higher by 46.81%, 71.05%, and 78.05%, respectively, than those of the unmodified aramid composites. The results showed that the IFSS of the aramid fiber was 16.24% higher than that of AF-20% KH550. The increase could be attributed to the growth of ZnO nanoparticles. The retention rate of the tensile strength of the unmodified aramid fiber was as low as 81.99% after 128 h of UV irradiation, and the retention rate of the aramid fiber after the growth of ZnO nanoparticles was 98.11%. The tensile, flexural, and compressive strength retention rates of aramid composites recorded following the surface growth of nano-ZnO were 98.08%, 91.49%, and 89.56%, respectively, which were significantly higher than the values recorded for unmodified aramid composites (82.19%, 75.44%, and 76.75%, respectively). The growth of nano-ZnO improved the UV resistance of aramid composites and the mechanical properties of aramid composites.

Keywords High performance · UV resistant · Weft-knitted composites · Interfacial properties · Mechanical properties

1 Introduction

Aramid is a high-performance fiber with excellent properties such as low density, high specific strength, and high specific modulus. It has received significant attention as an ideal reinforcement for polymer matrix composites [1]. Aramid-reinforced composites have been widely used in the fields of aerospace [2, 3], sports, fabrication of structural components [3], and electrical automation [4]. However, the lack of chemically active groups on the surface of aramid and the large number of amide bonds in the aramid macromolecular chain result in the poor UV resistance of aramid products. These properties also make forming an effective mechanical interlock with the resin matrix difficult. Weak interfacial bonds are formed under these conditions. Thus, aramid fibers have two inherent defects, low surface activity and poor UV resistance, which limit their development in the field of composite materials [5–8].

At present, the main anti-UV modification methods include inorganic nanocoating modification [9], organic polymer coating modification [10], organic polymer/inorganic nanocomposite coating modification, and spinning stock blend modification [11]. Zinc oxide (ZnO) stands out as a superb UV absorber with widespread application. ZnO nanoparticles exhibit remarkable high chemical activity, excellent catalytic properties, and resistance to both infrared and ultraviolet radiation. Nevertheless, the inherent weak chemical interaction between ZnO and fiber can lead to interfacial detachment, resulting in the deterioration or even failure of the composite material. Consequently, surface modification plays a pivotal role in enhancing the

✉ Cuiyu Li
licuiyu@tiangong.edu.cn

1 School of Textile Science and Engineering, Tiangong University, Tianjin, China

2 Key Laboratory of Advanced Textile Composites, Ministry of Education, Tiangong University, Tianjin, China

3 Nanjing Fiberglass Research & Design Institute Co., Ltd., Nanjing, China

interfacial bond strength of aramid fibers (AF). Several well-established surface modification techniques include chemical etching [12, 13], grafting [14–16], plasma treatment [17], γ-ray radiation [18], and electrochemical oxidation [19]. In pursuit of improved UV resistance, some scholars have undertaken approaches such as the growth of zinc oxide nanorods on the surface of aramid fibers and the modification of ultra-high-molecular-weight polyethylene (UHMWPE) fibers. The interfacial shear strength (IFSS) of the modified systems markedly exceeded that of unmodified aramid fibers, leading to substantial enhancements in UV resistance under these conditions [20–22]. Guan et al. [23] demonstrated enhanced UV resistance in aramid fibers by reacting surface-grafted chloride groups on para-aramid fibers with amino-octa-sesquisiloxane, a substance selectively absorbing UV light. This process resulted in the attachment of the amino-octa-sesquisiloxane units to the fibers via amide bonds.

Chemical modification surpasses physical modification in effectiveness by establishing stable chemical bonds, enhancing the reactivity of the fiber surface. Acid and alkali treatments, although effective, can lead to damage to aramid fibers. Conversely, Ca^{2+} ions in $CaCl_2$ exhibit the capacity to complex with amide groups coordinatively. Studies have demonstrated that this technique substantially reduces hydrogen bonding interactions and polymer crystallinity [24, 25]. Following $CaCl_2$ treatment, the fiber surface displayed increased roughness. However, the complex structure formed by $CaCl_2$ with the aramid fibers could not serve as a bridge between the fibers and the resin matrix [22], subsequent grafting of the silane coupling agent led to enhanced adhesion between aramid fibers and the resin [26]. Subsequently, ZnO nanoparticles bearing hydroxyl groups were grafted onto the surface through a dehydration reaction, and ZnO nanowires were further "grown" from the active seeds of ZnO nanoparticles on the AF surface. The functionalized AF exhibited enhanced UV resistance and improved interfacial properties with the matrix, resulting in increased interfacial strength. Knitted composites have garnered significant attention due to their superior impact resistance and energy absorption properties [27], weft-knitted composites offer excellent drape and formability, not only in the plane direction but also along the thickness direction, making them superior to other textile composites, including woven composites, in terms of mechanical properties [28]. In this study, a surface grafting approach was employed to modify aramid fibers and cultivate a layer of zinc oxide nanoparticles on the fiber surface, enhancing UV resistance without compromising fiber integrity. The modified aramid-based knitted fabric was used to reinforce the composite [29]. Simultaneously, mechanical properties of the reinforced composites and their UV resistance were thoroughly investigated.

2 Experiment

2.1 Materials

Aramid fibers (45tex) were purchased from DuPont. Acetone was sourced from Tianjin Jiangtian Chemical Technology Co., Ltd, China. Silane coupling agent KH550, sodium hydroxide, hydrochloric acid, zinc nitrate hexahydrate, hexamethylenetetramine, anhydrous calcium chloride were purchased from Tianjin Karees Fine Chemical Co., Ltd, China.

2.2 Functionalized Aramid Fibres and Aramid-Knitted Fabrics

10 wt% Anhydrous calcium chloride (solvent: anhydrous ethanol solution) and KH550 (a silane coupling agent) were first used to modify the surface of aramid fibers and fabrics, and a gradient of anhydrous ethanol solutions (KH550 mass fractions: 10%, 15%, 20%, and 25%) was used for the studies. The results revealed that the best results were obtained using a 20% ethanol solution. Based on this modification, solutions of NaOH (8 mmol/L; in anhydrous ethanol) and zinc acetate dihydrate (2.8 mmol/L; anhydrous ethanol solution) were prepared for the growth of ZnO. The two solutions were heated to 65 °C in a water bath. The zinc acetate solution was stirred vigorously while adding the NaOH solution, and the aramid fibers were immersed in the solution and dried in a vacuum oven for 30 min. The tests were repeated thrice. Subsequently, aqueous solutions of zinc nitrate hexahydrate, hexamethylenetetramine, and polyethyleneimine were prepared at 30, 28, and 4 mmol/L, respectively. The aramid fibers grafted with ZnO nanowires were immersed in the solution and heated in a water bath at 87 °C for 5 h. At the end of the process, the fibers were removed, washed with distilled water, and dried to obtain aramid fibers with ZnO nanowires grown on the surface (Fig. 1).

2.3 Preparation of Aramid Fiber-Reinforced Polymer

The UHMWPE fibers treated by the modification methods stated above were used to fabricate aramid fiber weft-knitted composites (Table 1). Aramid weft-knitted composites are manufactured using a vertical lay-up process with eight layers of fabric per composite, following the VARTM forming process (Fig. 2) [30]. Initially, eight layers of weft-knitted aramid fabrics are carefully arranged within the film cavity. Subsequently, a resin-curing agent

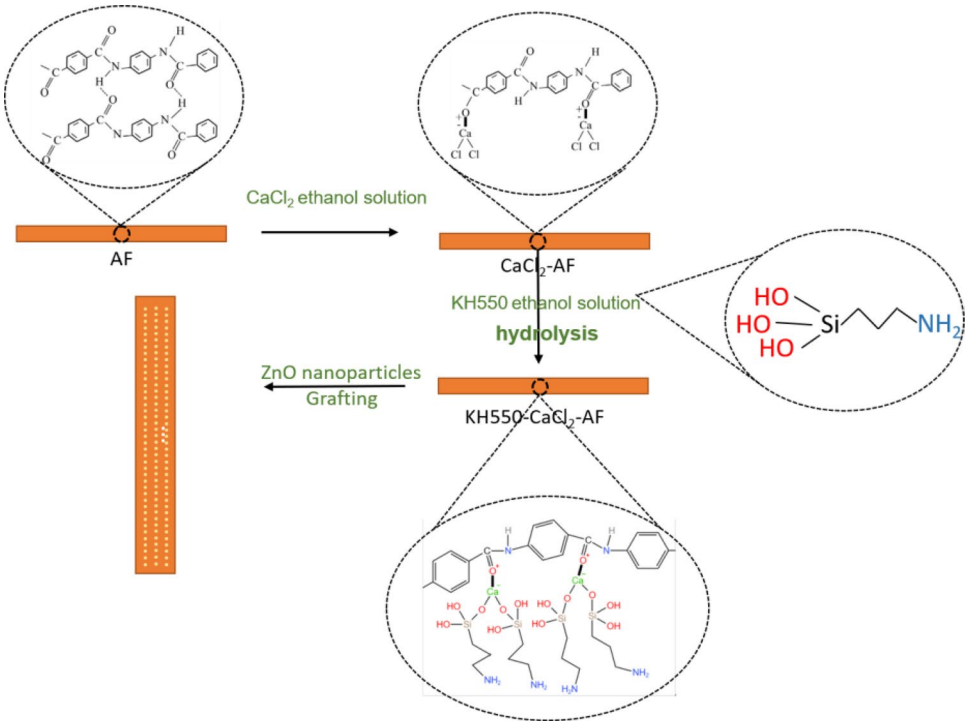

Fig. 1 The process of functionalized aramid fibers

Table 1 Parameters of weft-knitted composite materials

	Thickness *d* (mm)	Fabric layers	Fiber volume content V_f (%)	Transverse density (column/5 cm)	Vertical density (rank/5 cm)
Weft-knitted aramid knitted fabrics	2.65	8	47.82	40	32

mixture (Table 2) is prepared at a mass ratio of 10:3. This mixture is then injected into the sealed mold cavity under vacuum conditions, effectively impregnating the fibers. Following this, the film is allowed to cure and set for a period of 24 h at room temperature as illustrated in Fig. 3.

2.4 Characterization and Test Methods

2.4.1 Changes in the Surface Properties of Aramid Fibers

A bench-top scanning electron microscope (Phenom Pure, Fuhner Scientific Instruments, Eindhoven, The Netherlands) was used for analysis. The surfaces of the aramid fibers were observed before and after modification. A transform infrared spectrometer (Nicolet iS50, Thermo Fisher Ltd, USA) was also used for analysis. An X-ray photoelectron spectrometer (Thermo Scientific K-Alpha, ULVCA-PHI, Inc.) was used to record data to compare the changes in the functional groups on the surface of the aramid fibers before and after modification. The X-ray photoelectron spectrometer excitation source was Al Ka, the operating voltage was 12 kV, and the full spectral scan fluence energy was 150 eV (steps 1 eV). The contact angle was characterized with a contact angle meter (DSA30S, KRUSS Co., Ltd. Germany).

The tensile breaking strength of aramid filaments before and after modification was tested using an INSTRON 399 universal tensile tester (Strand Group, USA) at a loading rate of 2 mm/min. The test was performed according to the guidelines laid down in GB/T 19975-2005 Test Method for Tensile Properties of High Strength Chemical Fibre Filaments [31]. The final tensile strength of each group was obtained by averaging the data obtained over ten tests.

Interfacial shear strength test: The loading rate was 2 mm/min, and the final interfacial shear strength values for each group were obtained by averaging the data recorded by repeating the tests ten times.

IFSS determined following the pull-out test method could be used to characterize the fiber/matrix bond [32] (Fig. 4):

$$\mathrm{IFSS} = \frac{F_{\max}}{\pi dl} \tag{1}$$

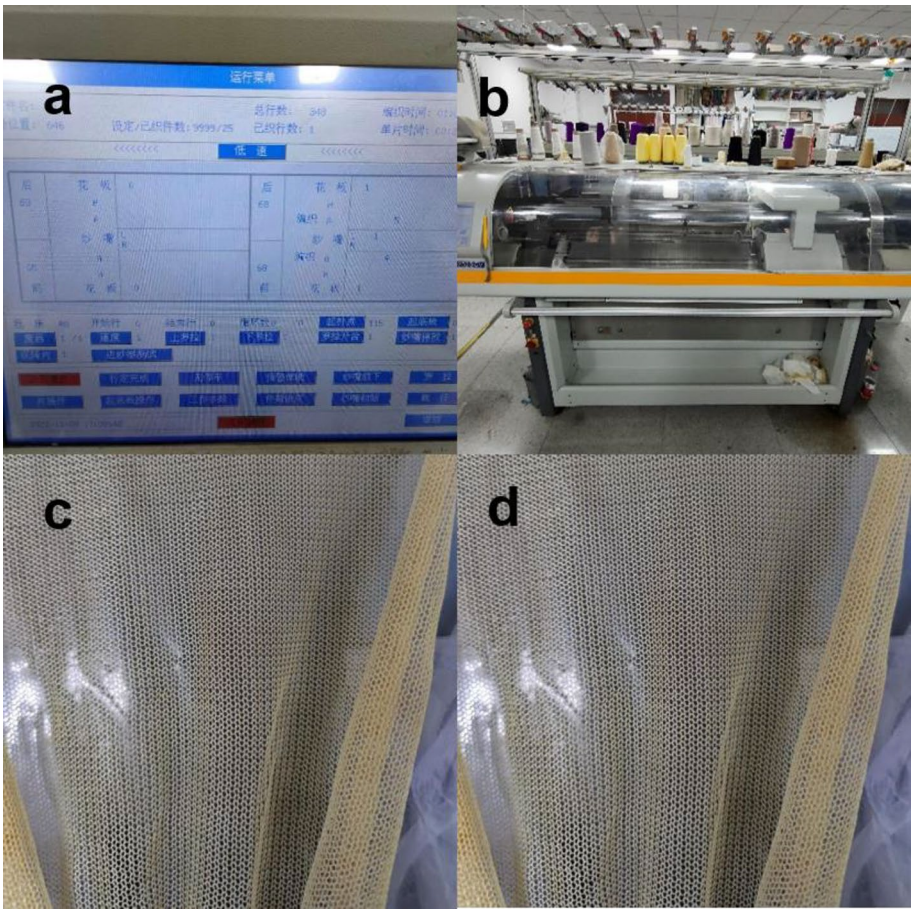

Fig. 2 **a** DSTW-01 digital small sample twisting combined machine. **b** Operation interface. **c** The front side of the fabric. **d** The reverse side of the fabric

Table 2 Parameters of epoxy resin and curing agent

	Epoxy resin GCC135	Hardener GCC135
Epoxy value (quantity/100 g)	0.54–0.6	–
Viscosity (Mpa s)	700–1100	10–50
Densities (g/cm^3)	1.13–1.17	0.93–0.98
Curing time	25 °C 24 h	

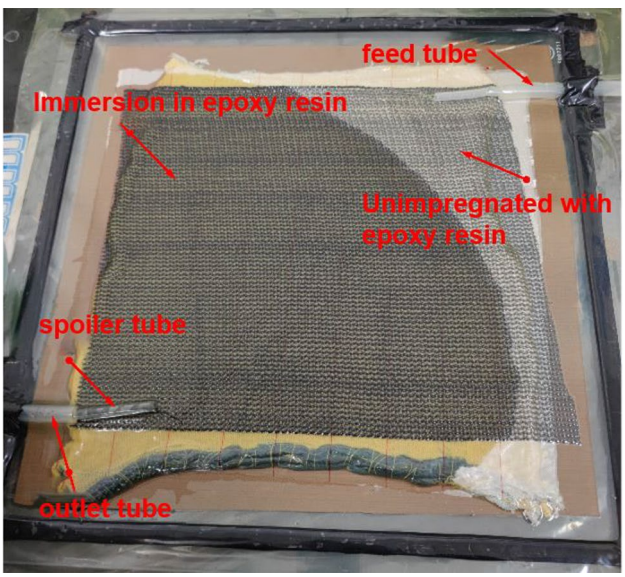

Fig. 3 The process of transferring resin under vacuum

2.4.2 UV Aging Fluorescence Testing

The properties of the aramid monofilaments and the aramid composites were studied before and after modification. A UV test for UV aging fluorescence testing (APLAS Material Testing Technology, USA) was used to irradiate the aramid fiber and its composite before and after UV aging modification. The standard ASTM G154 Cycle 1 was used during the experiment (i.e., the selected lamp type was UVA-340, the UV irradiance was 0.89 W/m^2 nm, the UV wavelength was 340 nm, and the black plate temperature was 60(± 3) °C).

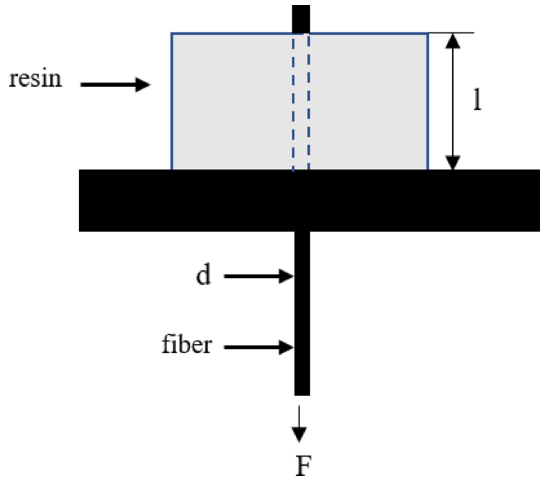

Fig. 4 Fiber extraction test model

2.4.3 Mechanical Testing of Composite Materials

The tensile, flexural, and compressive properties of the materials mainly reflect the mechanical properties of composite materials. The Instron 399 universal electronic tensile tester was used to conduct the tests. The loading rate was set at 2 mm/min.

(1) Tensile Properties

The tensile properties of aramid composites were tested using an electronic universal strength tester. The GB/T1447-2005 [33] guidelines were followed. The specimens were processed into dog-bone-shaped samples (Fig. 5).

(2) Bending Performance

The tests were conducted using GB/T1449-2005 [34].The composite laminate was cut into rectangular bending specimens, and the samples were tested following the three-point bending method under conditions of unrestrained support.

(3) Compression Performance

The guidelines in GB/T1448-2005 [35] were followed to conduct compression tests with aramid composites (Fig. 6). Four parallel specimens were used to obtain the mean and standard deviation of the properties of each material.

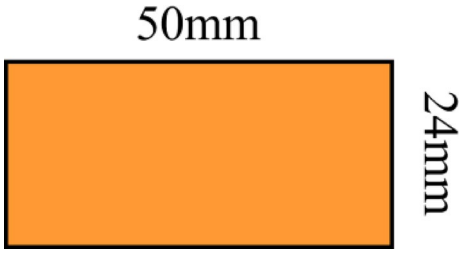

Fig. 6 Analysis of the rectangular specimens used to conduct compression tests

3 Results and Discussion

3.1 Micromorphology

Figure 7a presents the images recorded for the unmodified aramid fiber with a smooth surface containing small grooves. The surface of the aramid fiber in Fig. 7b was rougher compared to the surface of AF, and the generation of large grooves could be attributed to the complexation of the samples with a solution of $CaCl_2$. This resulted in the shedding of a part of the fiber skins. Figure 7c–f presents the surface morphology of the fibers modified with different concentrations of KH550. The higher the concentration of silane coupling agent, the better the grafting effect. But a large amount of fiver skin was shed when the concentration of KH550 was 25%. This resulted in fiber damage and the shedding of the layers of KH550, which were grafted successfully. The results revealed that the concentration of KH550 should be controlled at approximately 20%.

Figure 8 presents the morphology of the fibers treated with KH550 for prolonged time periods. Very little KH550 was left on the fiber surface after 7 h of treatment compared to 6 h of treatment. It can be concluded that a high extent of fiber skin peeling is observed under conditions of prolonged treatment time. The fiber gets damaged under these conditions. Therefore, the optimum treatment time should be controlled at approximately 5 h.

Fig. 5 Analysis of the dog-bone-shaped tensile specimen (mm)

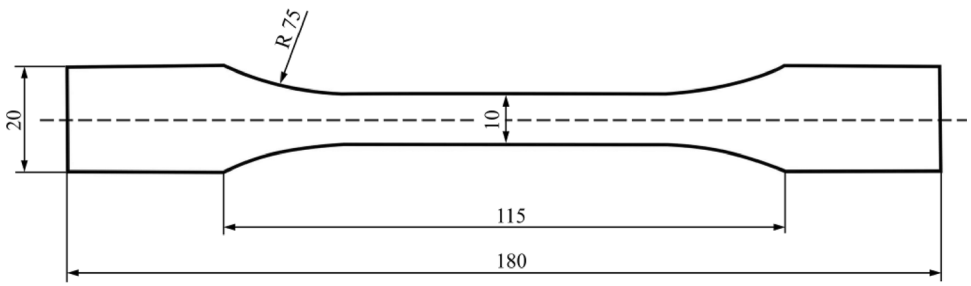

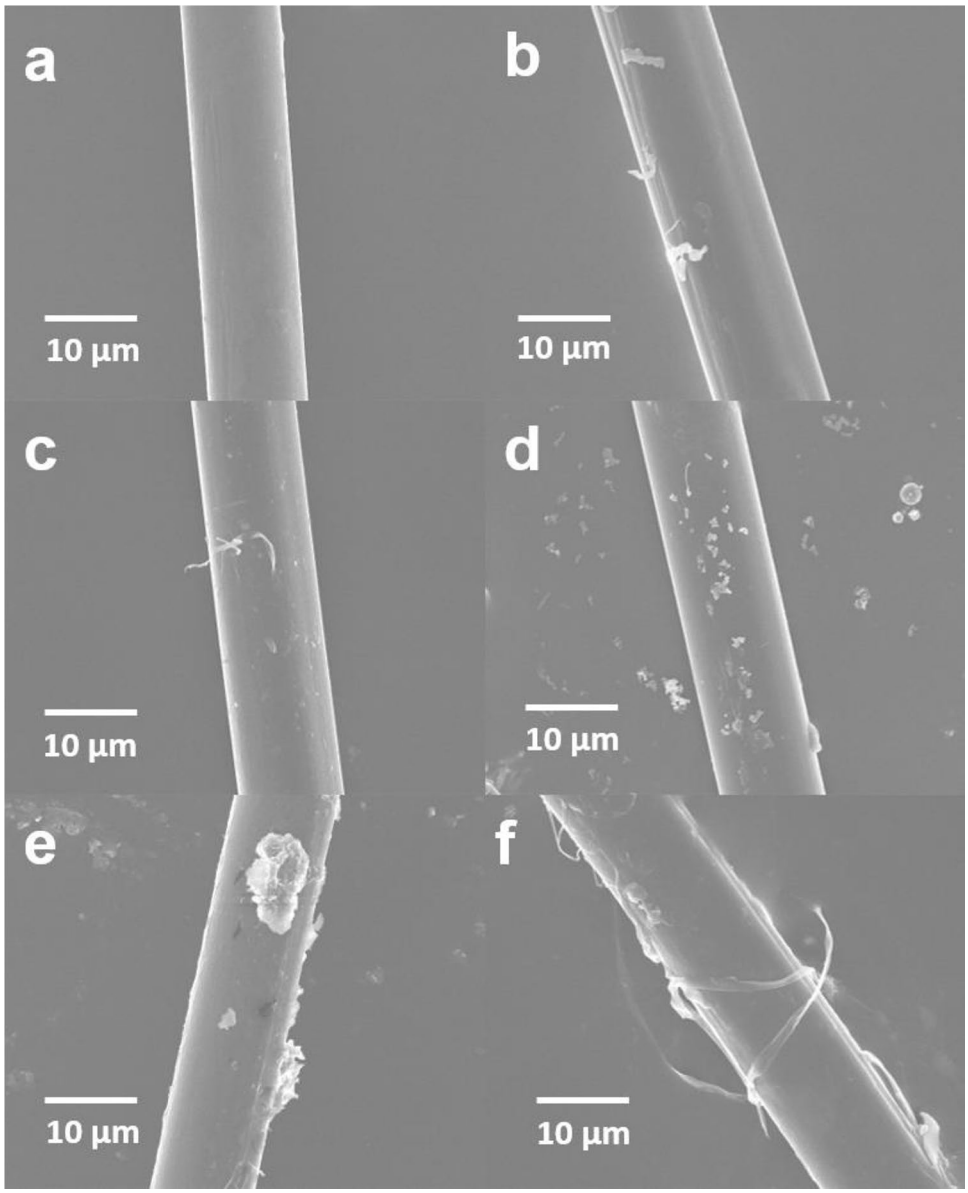

Fig. 7 Electron micrographs recorded for the surfaces of modified aramid samples to study the surface morphology of the samples: **a** unmodified aramid fibers; **b** $CaCl_2$-modified aramid fibers; **c** AF-$CaCl_2$-10%KH550; **d** AF-$CaCl_2$ 15%KH550; **e** AF-$CaCl_2$-20%KH550; **f** AF-$CaCl_2$-25%KH550

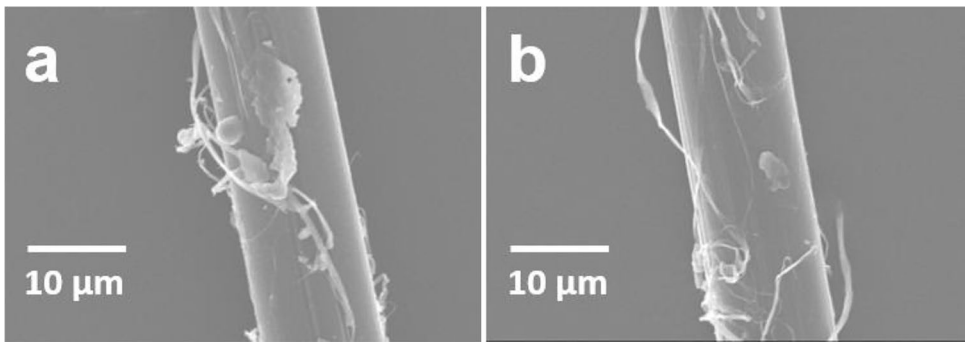

Fig. 8 Electron micrograph recorded for KH550 for the samples subjected to conditions of prolonged processing time: **a** 6 h; **b** 7 h

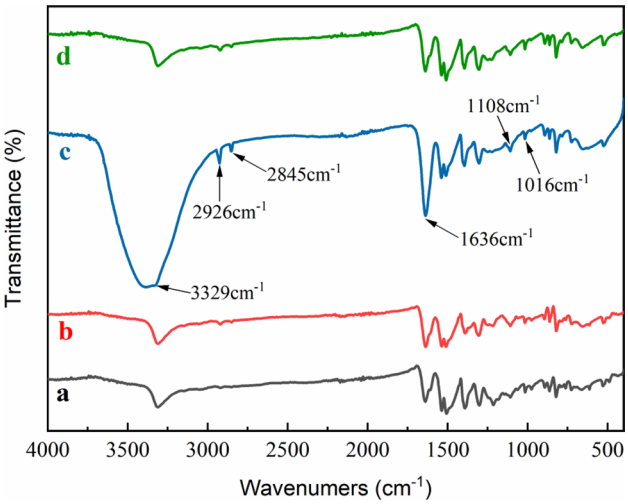

Fig. 9 FTIR spectral profiles recorded for aramid fibers before and after modification: **a** AF; **b** AF-$CaCl_2$; **c** AF-$CaCl_2$-KH550; **d** AF-g-ZnO NWs

Table 3 Elemental composition of AF surfaces of modified and unmodified samples

Sample	Elemental content (%)				O/C (%)
	C	O	Cl	Si	
AF	79.65	17.91	–	–	22.49
AF-$CaCl_2$	66.01	22.2	11.78	–	33.63
AF-$CaCl_2$_KH550	61.63	30.26	–	8.11	49.1

3.2 Analysis of the Surface Groups in the Fibers

Figure 9 presents the Fourier transform infrared spectrometer spectral profiles recorded for the surface of aramid fibers before and after modification. Subfigure (a) presents the profiles recorded for the unmodified aramid fibers, subfigure (b) presents the profiles recorded for the $CaCl_2$-treated aramid fibers, subfigure (c) presents the profiles recorded for the aramid fibers modified with both $CaCl_2$ and KH550, subfigure (d) presents the profiles recorded for the modified aramid fiber under conditions of the growth of ZnO nanoparticles. The C=O stretching vibration peak appears at 1636 cm^{-1}, the N–H stretching vibration peak appears at 3329 cm^{-1}, the N–H bending peak appears at 1540 cm^{-1}, and the C–N stretching peak appears at 1310 cm^{-1} in the profiles recorded for the original fiber. It can be seen that the positions of the characteristic peaks do not change significantly after $CaCl_2$ treatment and the intensity of the N–H stretching vibration peak at 3329 cm^{-1} increases slightly. The intensity of the N–H stretching vibration peak increases significantly when modified with KH550, and this proves that $CaCl_2$ and KH550 react with the amide bond on the aramid fiber to form large amount of N–H bonds. The absorption peaks at 2926 and 2845 cm^{-1} correspond to the asymmetric and symmetric stretching vibrations, respectively, of the methylene group. The peak corresponding to the C–Si group appeared at 1108 cm^{-1}, and the stretching vibration peak of the C–O–Si bond appeared at 1016 cm^{-1}. These characterizations demonstrate the successful grafting of KH550 onto the surface of the aramid fibers and the introduction of a large number of reactive oxygen-containing groups on the sample surface. The curves in (d) are less intense than those in (c). It was observed that the positions of the characteristic peaks remained almost unchanged, demonstrating the successful growth of the nano-ZnO units which covered the surface of the fibers.

3.3 Elemental Content Analysis

Table 3 presents the elemental composition of the aramid surfaces before and after modification, and Fig. 10 presents the XPS profiles recorded for the aramid fiber surfaces. The carbon-to-oxygen ratio indirectly reflects the content of oxygen-containing groups. As can be seen from the graphs, after treatment with $CaCl_2$, the concentration of Cl and O increased, while the concentration of C decreased. This

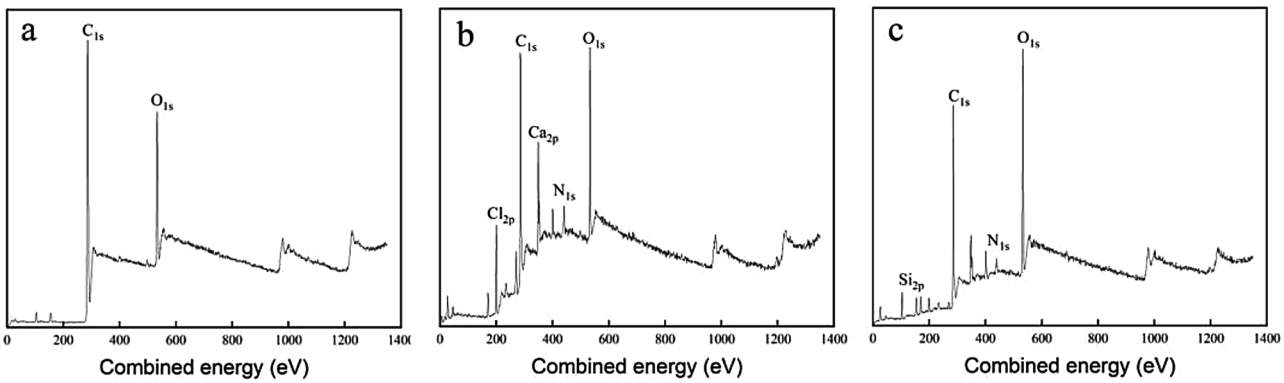

Fig. 10 XPS profiles recorded for **a** AF; **b** AF-$CaCl_2$; **c** AF-$CaCl_2$-KH550

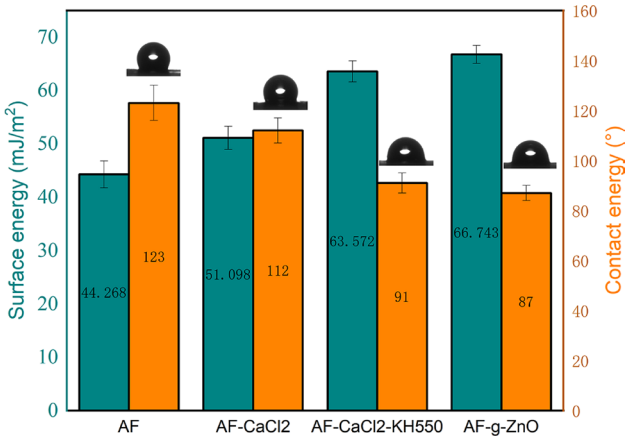

Fig. 11 Contact angle and surface energy values recorded for modified and unmodified aramid fibers

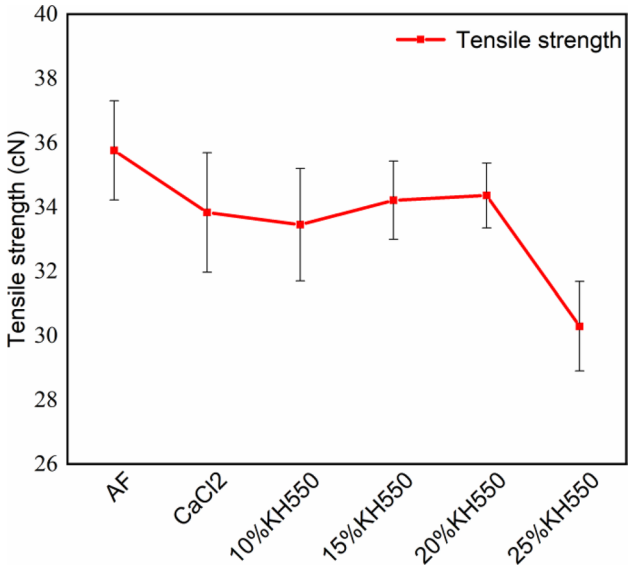

Fig. 12 Tensile strength of the modified and unmodified samples

confirmed that $CaCl_2$ reacted with the amide group in aramid, and this resulted in the introduction of Cl on the fiber surface. The oxygen-to-carbon ratio was 33.63%. The concentration of elemental O continued to increase while the concentration of C continued to decrease when the samples were treated with KH550. This confirmed the successful grafting of KH550 onto the fiber surface and the increase in the carbon-to-oxygen atomic ratio from 22.49 to 49.1%. The increase in ratio could be attributed to the fact that KH550 was rich in oxygen-containing functional groups. The increase in oxygen concentration on the fiber surface resulted in increased surface activity and improved interfacial properties.

3.4 Fiber Wetting Performance

The interfacial properties of aramid units in textile composites are closely related to the property of interfacial wettability, which is reflected by the contact angle and surface free energy values (Fig. 11). The contact angle for AF was recorded to be 123°, and the surface of AF was extremely hydrophobic. The hydrophobicity decreased with the progress of the modification progresses. The degree of wettability of the aramid surface increased gradually. It was observed that the surface free energy associated with AF-$CaCl_2$-20% KH550 increased significantly from 44.268 to 63.572 mJ/m^2. Despite the introduction of hydrophilic groups under conditions of $CaCl_2$ treatments, the contact angle could be reduced by 112°, and the surface free energy could be increased by 51.098 mJ/m^2. This indicated limited increase in the degree of wettability of the aramid units. However, the corresponding decrease and increase in these parameters were 18.75% and 24.41%, respectively, when KH550 was subsequently introduced. These apparent changes indicate that grafting KH550 onto the surface of the aramid significantly improved the degree of wettability of the aramid fibers. The surface growth of ZnO nanoparticles improved the fiber surface properties, indicating that zinc oxide nanoparticles have improved the wettability of aramid surfaces.

3.5 Fiber Tensile Strength Tests

The tensile breaking strength of the fiber directly affects the ability of the fabric to absorb energy. This helps maintain the level of tensile strength, and this is critical to maintain the effectiveness of the interfacial modification method [36].

It has been reported herein that the breaking strength of the modified aramid monofilament was slightly lower than that of the virgin aramid, and the retention rate was approximately 95% (Fig. 12). The breaking strength of the AF-$CaCl_2$-20% KH550 was 34.36 cN, and the retention rate was 96.09%. The tensile strength of the modified aramid fibers tended to decrease under complexation conditions. The decrease could also be attributed to the slight peeling of the fiber skin. The tensile strength increased when the KH550 concentration was 15%, and this could be attributed to the fact that KH550 adhered to the surface of the aramid fibers. Moreover, it functioned as a binder that bonded with the surface of the sample during the fiber modification process. The load capacity increased to a small extent when the samples were stretched. The maximum tensile breaking strength of the modified fiber was obtained at a KH550 concentration of 20%. However, the tensile strength of fibers dropped significantly when the KH550 concentration reached 25%. The results revealed that a significantly high concentration of the modifying reagent damaged the aramid fiber. Therefore, the

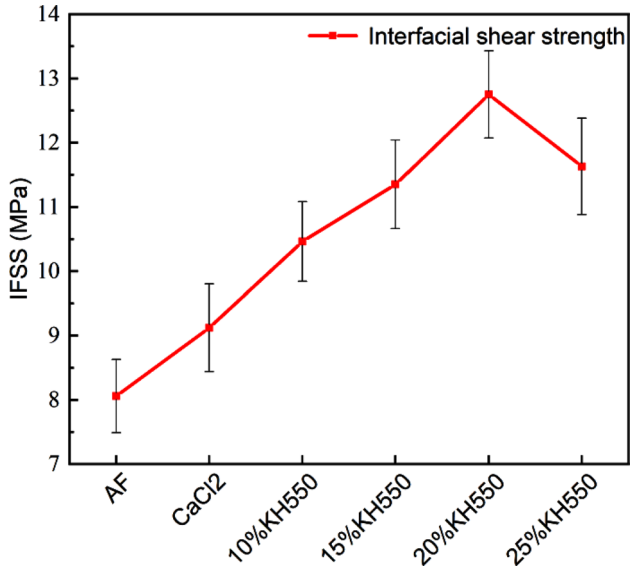

Fig. 13 Interfacial shear strength of the modified and unmodified samples

optimum KH550 concentration for treatment was identified to be 20%.

3.6 Analysis of Fiber Interfaces Through Shear Strength Tests

Aramid filament pull-out tests were carried out to assess the interfacial properties of the modified aramid fibers, and the results are shown in Fig. 13. IFSS reflects the efficiency of load transfer at the fiber/resin interface. The IFSS values recorded for the modified aramid monofilaments were significantly higher than those recorded for the unmodified aramid systems. The surface of the untreated aramid fiber was smoother than the surface of the treated fiber, and less friction was realized under conditions of debonding when the fibers slid against the substrate. The surface was inert, and a sufficient number of binding sites were not present at the interface of the fiber and the substrate. As a result, the fibers could be readily pulled out. The 13.15% increase in IFSS of AF-$CaCl_2$ (compared to the IFSS of the original fiber) indicated that the interfacial adhesion property between the fiber and the resin could be improved. The results also revealed that calcium chloride formed a graft layer on the fiber surface, increasing the degree of surface roughness and wettability of the aramid fibers.

When grafted with KH550, the graft layer covers the smooth surface, increasing the surface roughness. The reactive functional groups on the grafted layer react with the silicone hydroxyl and epoxy groups of KH550 through chemical bonding or physical interaction. This results in the generation of an interlocking effect [37, 38]. The results revealed that the grafting of KH550 resulted in a significant improvement in the IFSS value at the interface. The maximum IFSS was recorded when the KH550 concentration was 20%, and the IFSS of the AF-$CaCl_2$-20% KH550 sample was 58.19% higher than that recorded for the unmodified aramid fibers. The results of the SEM images combined with analysis of the pull-out tests show that a large amount of KH550 was shed along with the aramid skin, bare aramid fibers which tended to slip when forming an interface with the epoxy matrix. Thus, a further increase in the concentration of KH550 would not only negatively affect the strength of the aramid fiber but also exert a major impact on the interfacial shear strength of the materials.

3.7 Characteristics and UV Resistance of Samples

3.7.1 Surface Morphology

Figure 14 presents the electron micrographs of aramid fibers containing ZnO nanoparticles on the surface. The ZnO nanoparticles were successfully grown on the surface of the aramid fibers, and these nanoparticles formed a dense ZnO coating. The aggregation of ZnO nanoparticles on the surface increased the roughness of the surfaces. The increase in surface roughness could also be attributed to the direct attachment of part of ZnO nanoparticles to the KH550,

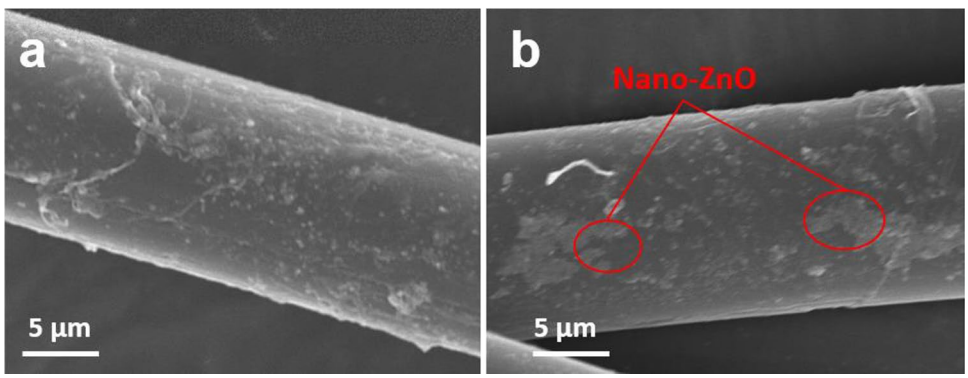

Fig. 14 Electron microscopy images recorded for aramid fibers containing surface-grown ZnO nanoparticles

Table 4 Elemental composition corresponding to AF surfaces recorded before and after modification

Sample	Elemental content (%)				O/C (%)
	C	O	Zn	Si	
AF	79.65	17.91	–	–	22.49
AF-$CaCl_2$-KH550	61.63	30.26	–	8.11	49.1
AF-g-ZnO NWs	58.72	29.85	6.26	5.17	50.83

which resulted in the formation of blocks on the sample surface.

3.7.2 Elemental Content Analysis

Table 4 presents the elemental composition of the surface of the grown ZnO nano-aramid fibers, and Fig. 15 presents the XPS profiles recorded for the fiber surface. The elemental content of Zn on the fiber surface was 6.26%, and the elemental content of Si was reduced from 8.11 to 5.17% following the growth of ZnO nanowires on the sample surface. The results proved that ZnO nanowires enveloped the aramid surface. The O content of the aramid surface did not change significantly after the introduction of the ZnO nanowires, but the C content decreased due to the reduction of the exposed area of the aramid surface under the conditions of homogeneous ZnO wrapping. The increase in the oxygen/carbon ratio to 50.83% and the increase of the proportion of oxygen-containing groups also contributed to the results.

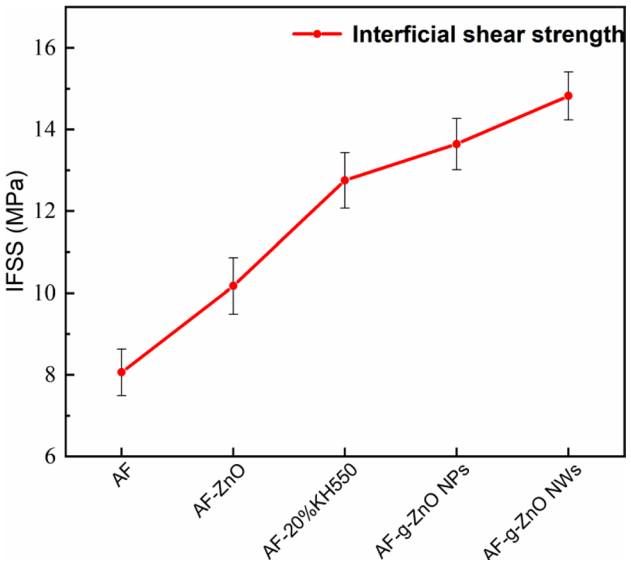

Fig. 16 Shear strength test chart for fiber interfaces

3.7.3 Analysis of Fiber Interface and Determination of the Shear Strength

Figure 16 shows the interfacial shear strength of aramid fibers after growing ZnO nanoparticles. A control experiment was conducted to verify the modified aramid fibers on the interfacial shear strength (IFSS) of aramid fibers. In this experiment, AF-ZnO was directly synthesized on the surface of aramid fibers without any prior treatment involving calcium chloride and KH550, following ultrasonic cleaning of the aramid fibers. As depicted in the graph, the IFSS experiences a significant enhancement post KH550 modification, underscoring the pivotal role of KH550 in enhancing

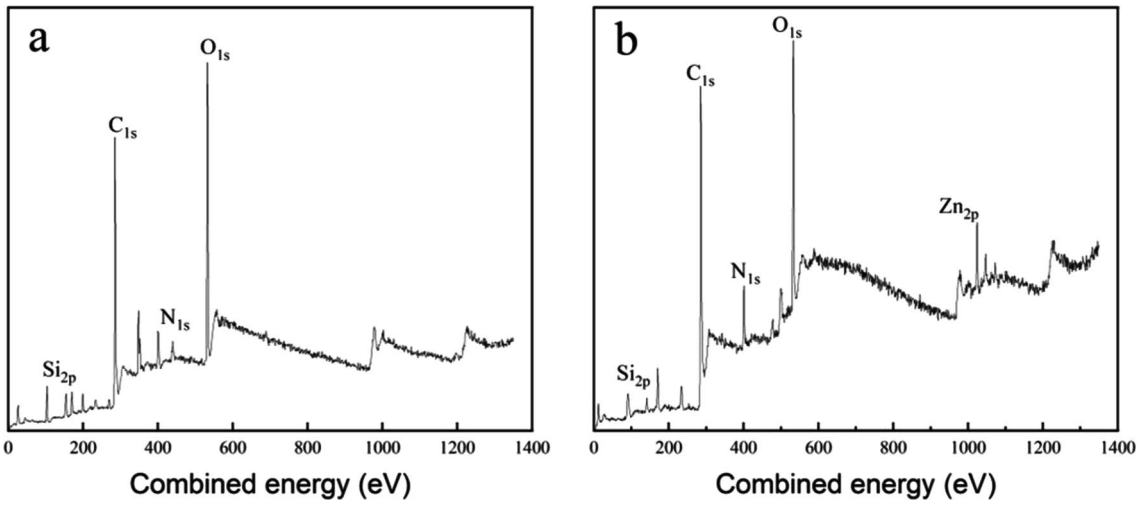

Fig. 15 XPS profiles recorded for **a** AF-$CaCl_2$-KH550 and **b** AF-g-ZnO NWs

aramid fiber wettability. Upon modification of aramid fibers with calcium chloride and KH550, and growing followed by the growth of ZnO nanowires, the IFSS of AF-g-ZnO NWs rose to 14.82 MPa. This represented a substantial increase of 45.72%, 16.24%, and 83.87% when compared to AF-ZnO, AF-20% KH550, and AF, respectively. These results unequivocally demonstrate that the growth of nano-ZnO significantly enhances the UV resistance of aramid fibers and augments their surface activity. Moreover, it highlights the critical role of KH550 in aramid wettability. The combined use of KH550 modification and nano-ZnO is the only effective approach for significantly enhancing. Furthermore, the concurrent utilization of KH550 modification and nano-ZnO emerges as the sole effective strategy for substantially bolstering both the wettability and UV resistance of aramid fibers.

3.7.4 Analysis of the Mechanical Properties of Fibers Not Subjected to and Subjected to UV Irradiation

The poor UV resistance of aramid fibers can be attributed to the vulnerability of the amide bonds in their molecular structure, which undergoes decomposition upon exposure to UV irradiation. ZnO nanoparticles are used to address this issue due to their ability to shield against UV radiation. The shielding effect of ZnO is primarily achieved through the absorption and scattering of UV radiation. In the near-UV region, ZnO primarily converts UV radiation into heat through electronic excitation and bonding [39, 40]. The UV resistance of the aramid fibers was assessed by evaluating their tensile strength retention after UV aging. The UV resistance of the aramid fibers was primarily indicated by the extent to which their tensile strength was preserved following exposure to UV-induced aging.

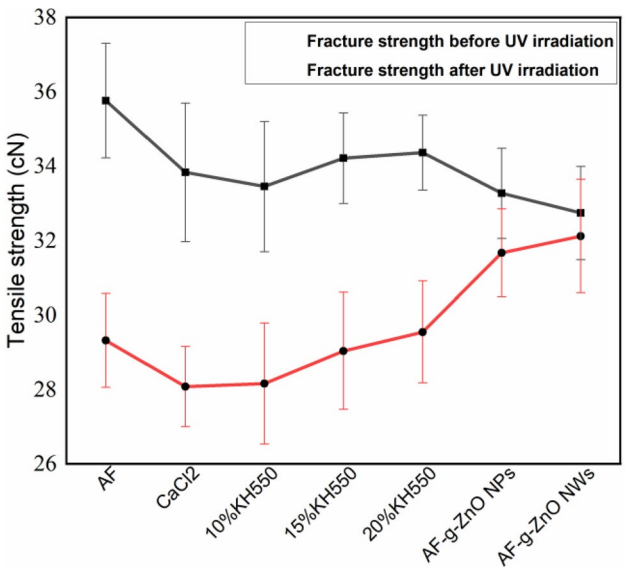

Fig. 17 Comparison of the breaking strength of aramid fibers not subjected to and subjected to UV irradiation

Figure 17 presents a comparison of the breaking strengths of aramid fibers before and after undergoing UV aging for a duration of 128 h. The initial tensile strength of unmodified aramid fibers was 35.76 cN, which decreased to 29.32 cN following UV irradiation, resulting in a retention rate of 81.99%. For the modified aramid fibers, the tensile strength retention rate increased as the concentration of KH550 increased. Among the modified fibers, aramid fibers with ZnO nanoparticles (AF-g-ZnO NPs) exhibited significantly higher tensile strength retention, with a retention rate of 95.19%. Furthermore, aramid fibers with ZnO nanowires grown on the surface (AF-g-ZnO NWs) demonstrated a tensile strength of 32.74 cN before UV irradiation, which slightly decreased to 32.12 cN after UV exposure. This resulted in a retention rate of 98.11%. These findings demonstrate the ability of ZnO nanoparticles to enhance the UV resistance of aramid fibers.

3.8 Aramid-Reinforced Composite Laminates

3.8.1 Analysis of Tensile Properties

Figure 18a, b illustrates that the tensile strength and tensile modulus of the modified aramid composites exhibit improvements compared to the unmodified composites. The $CaCl_2$-treated composites showed a 13.78% increase in tensile strength compared to the original composites, although this increase was not particularly significant. Following KH550 treatment, both the tensile strength and tensile modulus of the composites increased as the concentration of KH550 increased. Among the KH550-modified aramid composites, the highest mechanical properties were achieved with the 20% KH550 modification. The tensile strength and tensile modulus of these composites were measured at 110.27 MPa and 7051.39 MPa, respectively. These values were 46.81% and 38.65% higher than those of the original composites.

The curves depicted in Fig. 18c initially exhibit a linear upward trend. As the axial deformation increases, the resin matrix begins to fracture. The bonding capacity between the modified aramid and the resin matrix enhances, resulting in an increase in stress. As deformation continues, the resin matrix experiences further breakage, and the aramid coils start to debond and slide against the resin matrix, causing the curve to flatten. The extent of curve flattening is influenced by the fiber surface modification, which affects the debonding and sliding process. At a certain level of deformation, the resin matrix is completely fractured, and the fabric coils, having reached their maximum strength, break entirely across the cross-section. This results in a sharp drop

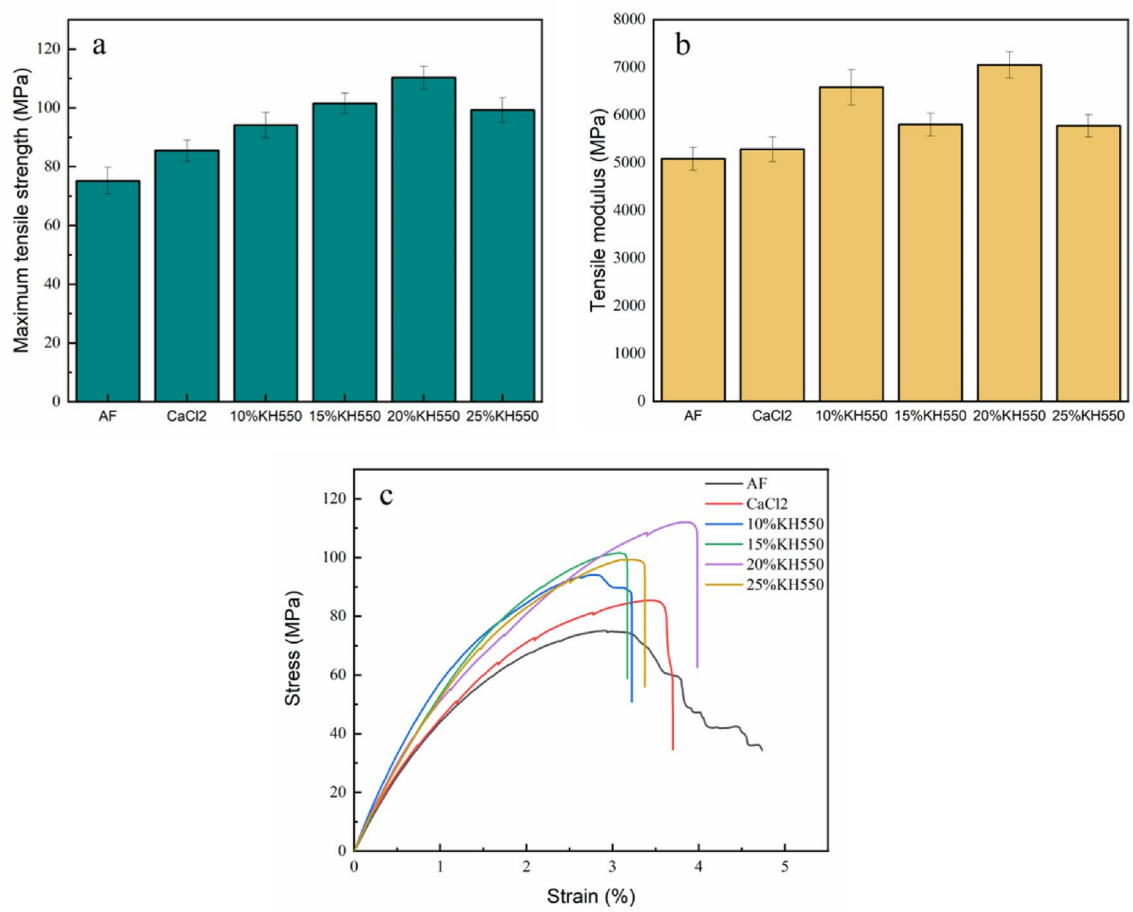

Fig. 18 Tensile test data recorded for aramid composites before and after modification: **a** maximum tensile strength; **b** tensile modulus; **c** stress–strain curves

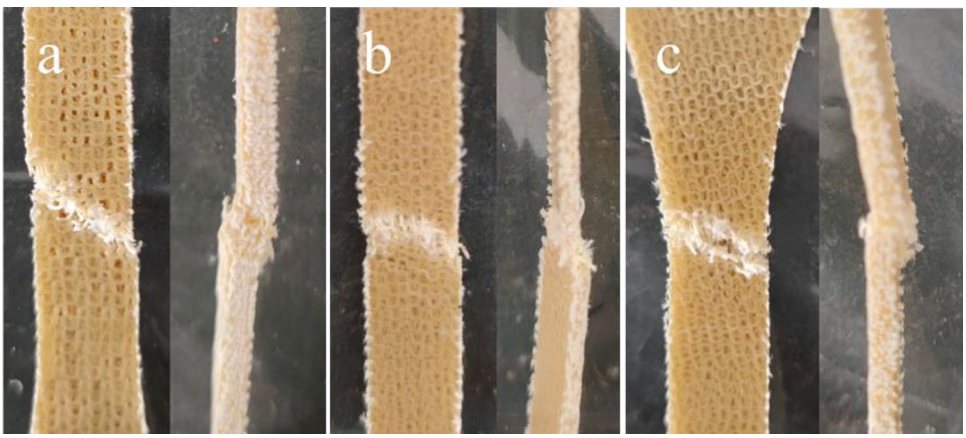

Fig. 19 Front and side tensile damage diagrams for aramid composites before and after modification: **a** AF; **b** AF-$CaCl_2$-20%-KH550; **c** AF-g-ZnO

in the curve. Notably, the curve of the unmodified aramid composite does not decline steeply but gradually decreases. This can be attributed to the smooth surface of the aramid fibers and the slipping of the fibers after the resin matrix breaks, occurring as the load displacement increases. These observations further support the notion that the modification of aramid fibers has significantly enhanced the mechanical properties of the composites [26, 41].

Figure 19 presents the tensile damage diagrams of the front and side of the composite, both before and after modification. On the fracture surface of the aramid composite, numerous fibers can be observed being pulled out. During

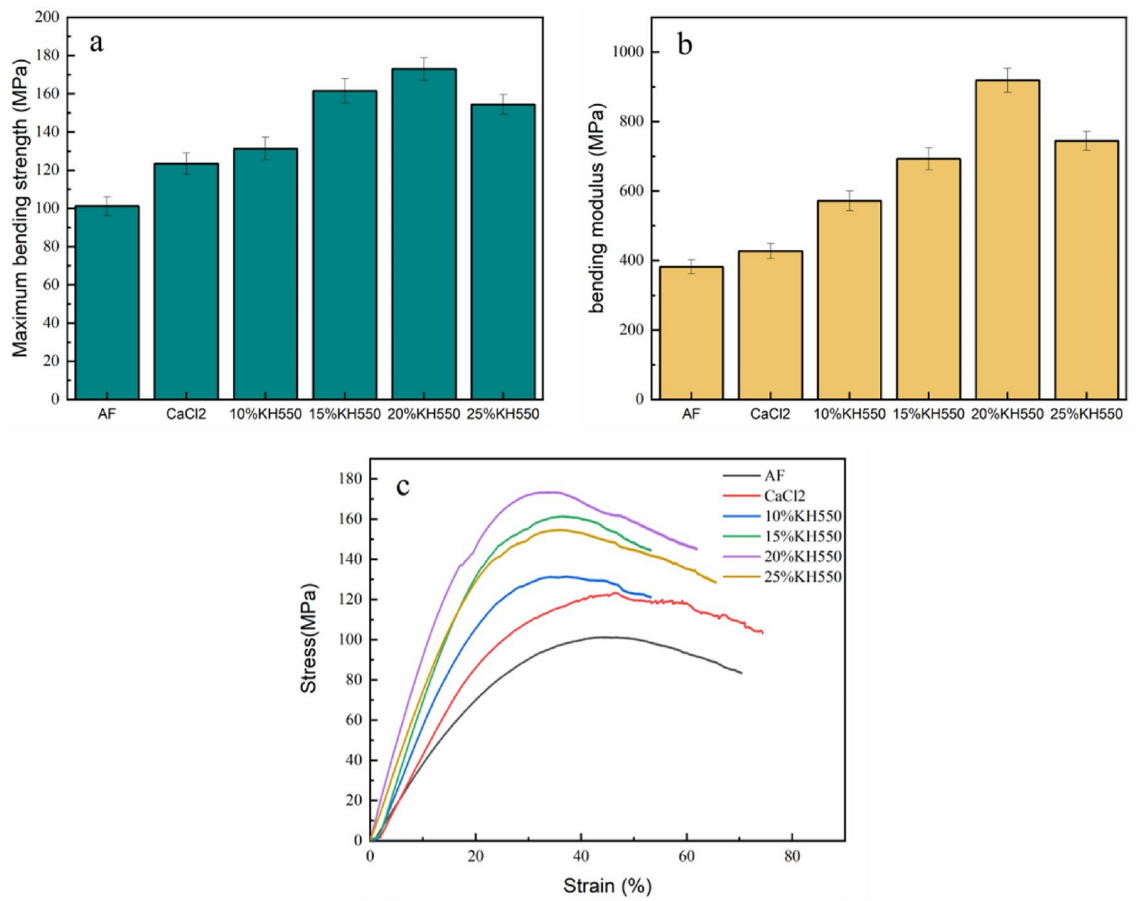

Fig. 20 Bending test data for aramid composites recorded before and after modification: **a** maximum bending strength; **b** bending modulus; **c** stress–strain curve

the stretching process, the resin matrix initially undergoes distributed cracking, and fiber debonding occurs due to the weak bond between the fibers and the matrix. Eventually, some of the fibers break while others are pulled out. As the concentration of KH550 increases, the number of pulled-out fibers decreases, and the elongation at break diminishes compared to the unmodified composite. This indicates that the bond between the modified aramid and the epoxy resin strengthens.

3.8.2 Analysis of Bending Performance

Figure 20a, b demonstrates that the flexural properties of the composites improve as the concentration of the silane coupling agent KH550 increases. The composites modified with 20% KH550 exhibit the maximum flexural strength and flexural modulus, measuring 173.08 MPa and 918.98 MPa, respectively. These values are 71.05% and 140.65% higher than those of the unmodified composites, and 40.29% and 115.05% higher compared to the $CaCl_2$-modified composites. The increased surface activity and roughness of the aramid fibers result in enhanced bonding with the epoxy resin and increased friction. Consequently, when the composite is subjected to bending, the extent of deformation of the aramid fibers decreases, resulting in increased stiffness. During the initial stage, the resin matrix experiences a higher load, causing the curve to rise with a steeper slope (Fig. 20c). As the resin matrix starts to fracture, the aramid assumes a greater portion of the load, causing the curve to flatten and the slope to decrease due to the ductility of the fabric coils. When the maximum load capacity is reached, slippage or even fracture occurs between the aramid and the resin matrix, leading to a decline in the curve.

3.8.3 Analysis of Compression Performance

Figure 21a, b presents histograms depicting the maximum compressive strength and compressive modulus of the composites, respectively, before and after modification. The composites modified with 20% KH550 exhibit a compressive strength of 21.31 MPa and a compressive modulus of 328.45 MPa. These values are 78.76% and 110.54% higher

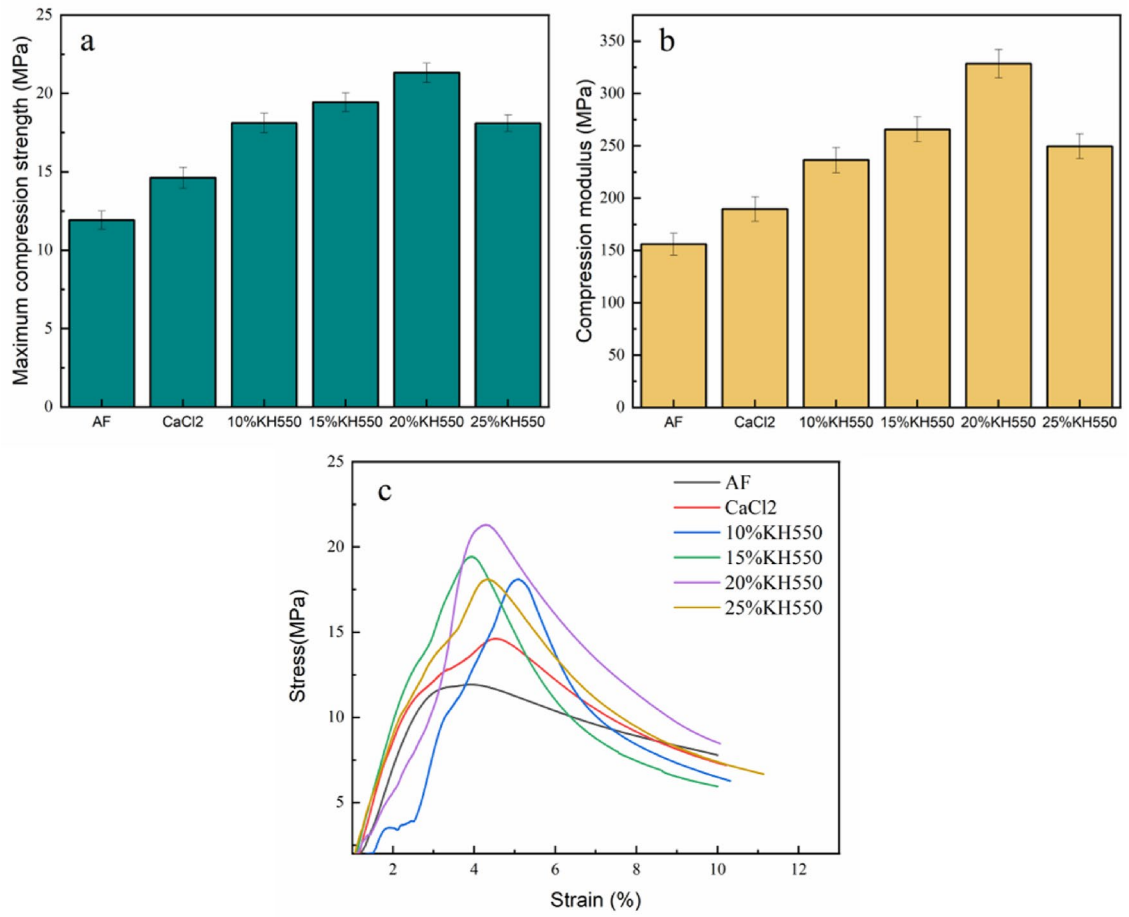

Fig. 21 Graph of compression test data for aramid composites before and after modification: **a** maximum compression strength; **b** compression modulus; **c** stress–strain curves

than those of the unmodified composites, and 45.83% and 73.21% higher than the $CaCl_2$-modified composites, respectively. In Fig. 21c, the curve exhibits a sharp upward trend during the initial stage. The material experiences minimal deformation at this point, and the resin matrix primarily bears the load. As the load displacement reaches a certain point, the resin matrix and fabric reinforcement share the load, resulting in a stronger fabric deformation capacity. The curve then gradually rises as the composite material undergoes noticeable deformation. Finally, when the maximum stress is reached, the composite material starts to experience damage, leading to a decline in the curve. The improved bonding of the modified aramid fabric to the resin matrix contributes to an increased stiffness of the composite material.

3.8.4 Comparison of the Tensile Properties Studied Before and After UV Exposure

Figure 22 provides a comparison of the tensile properties of the aramid composites before and after UV irradiation. Histograms (a) and (b) display the maximum tensile strength and tensile modulus, respectively. After 128 h of UV irradiation, the unmodified composite exhibited a tensile strength of 61.73 MPa, with a retention rate of 82.19% compared to the composite without UV irradiation. In contrast, the aramid composite modified with KH550 demonstrated a higher tensile strength retention rate of 88.35% due to the adherence of KH550 to the surface of the aramid fabric, which acted as a shield for the aramid itself. The aramid composite with ZnO nanowires on the surface displayed a tensile strength of 112.04 MPa, with a retention rate of 98.08%, significantly surpassing the original composite's retention rate of 82.19%. Notably, the tensile strength of the aramid composite with ZnO nanowires, without UV irradiation, was 114.23 MPa, which was 3.59% higher than that of the 20% KH550-modified composite. It is evident that the growth of ZnO nanowires not only greatly enhanced the UV resistance of the aramid composites but also improved their mechanical properties.

From Fig. 22b and c, it is evident that the tensile modulus of the composite decreases after UV irradiation. The

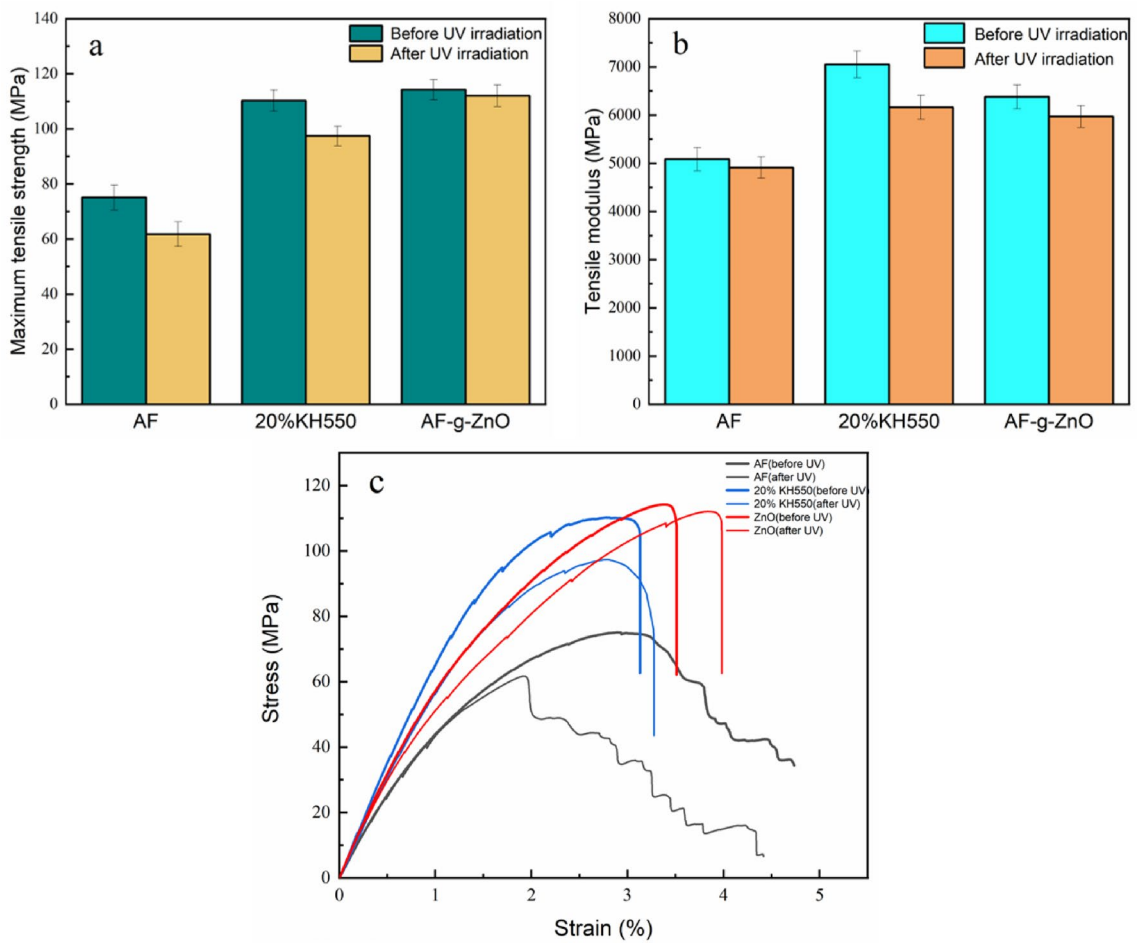

Fig. 22 Comparison of tensile test data recorded for aramid composites before and after UV irradiation: **a** maximum tensile strength; **b** tensile modulus; **c** stress–strain curves

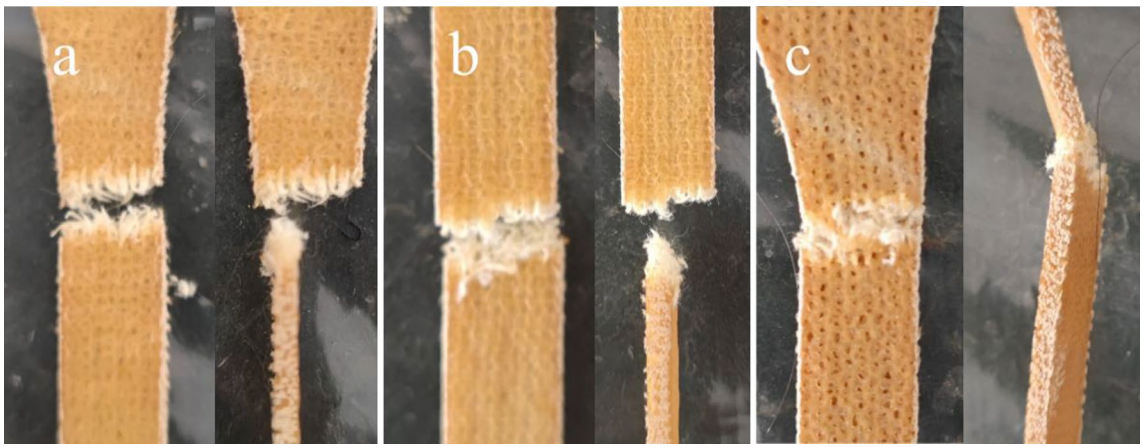

Fig. 23 Frontal and lateral tensile damage of aramid composites subjected to UV aging: **a** AF; **b** 20%KH550; **c** AF-g-ZnO

stress–strain curves exhibit a similar shape, indicating that the properties of the composite itself are not significantly altered. However, the mechanical properties of the aramid fabric itself are reduced after UV irradiation, leading to decreased bonding properties between the aramid and the resin matrix. This reduction is reflected in the curve's slope

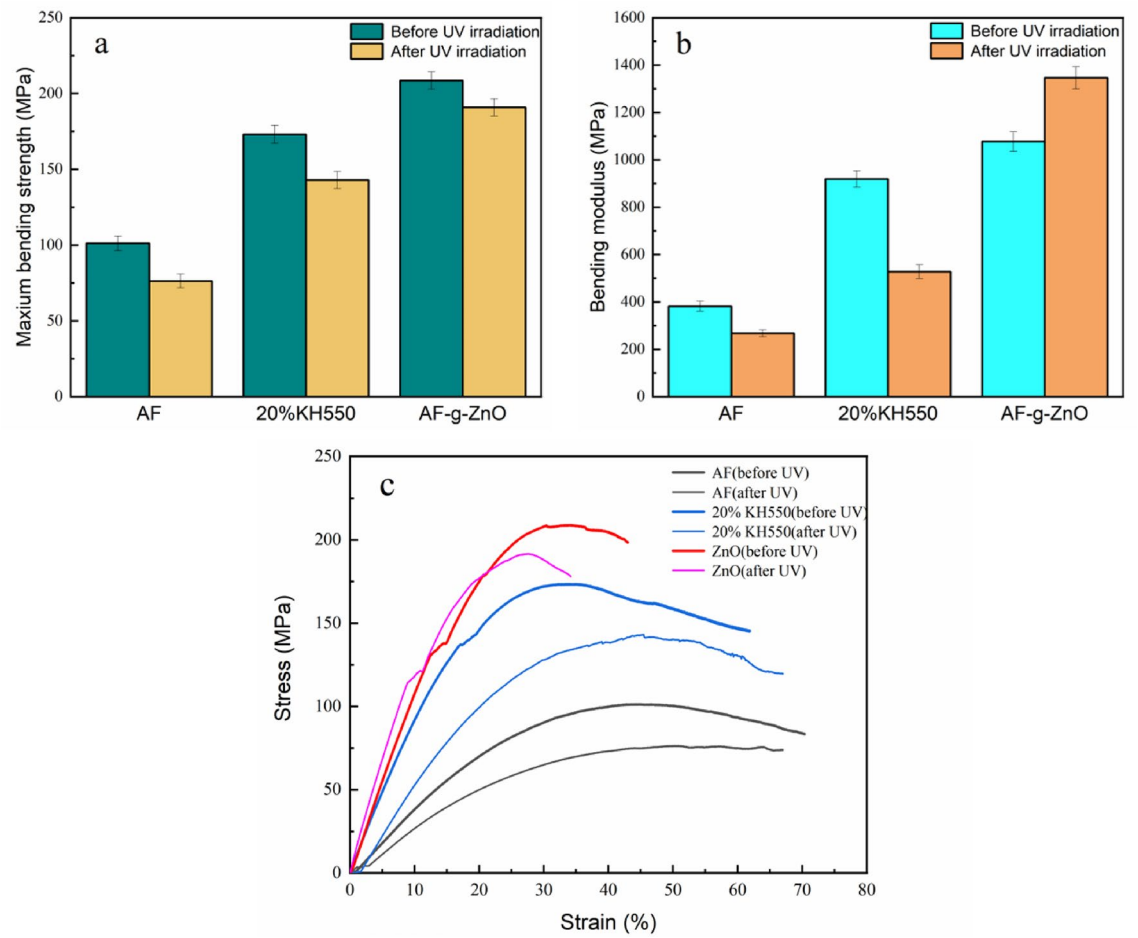

Fig. 24 Comparison of bending test data recorded for aramid composites before and after UV irradiation: **a** maximum bending strength; **b** modulus of bending; **c** stress–strain curves

and stress. Figure 23 illustrates that the number of fibers pulled out increases, and the fracture surface of the composite matrix appears flatter after UV irradiation. UV radiation has a greater impact on the aramid fibers, causing direct fracture of the composite. The difference between composites with surface-grown ZnO nanoparticles and those subjected to UV irradiation is not substantial. This indicates that UV irradiation affects the mechanical properties of the composites, while the growth of ZnO nanoparticles proves effective in preventing the loss of mechanical properties in the composites.

3.8.5 Comparison of Flexural Properties Studied Before and After UV Exposure

Figure 24a and b reveals the flexural strength retention of the unmodified aramid composite after UV irradiation to be 75.44%. The composite modified with 20% KH550 exhibited a flexural strength retention of 82.56%. However, the flexural modulus was reduced by 42.59%. This reduction may be attributed to the impact of UV radiation on the epoxy resin, causing the resin to yield more easily and resulting in a decrease in the composite's stiffness. In the case of the aramid composite with ZnO nanowires grown on the surface, the flexural strength after UV irradiation reached 190.83 MPa with a remarkable retention rate of 91.49%. This high retention rate can be attributed to the absorption and reflection of UV by the ZnO nanowires, effectively preventing damage to the aramid fabric caused by UV exposure. In Fig. 24c, the curve direction of the same specimen before and after surface UV irradiation remained largely consistent. There was an increase in strain when the maximum stress was reached, and a slight change in the composite material's yield point. The curve began to decrease gradually after reaching the yield point. However, the changes in the curve slope, yield point, and flexural modulus of the aramid composites with surface-grown ZnO nanowires differed from the aforementioned observations. These differences could be attributed to experimental errors during the testing process.

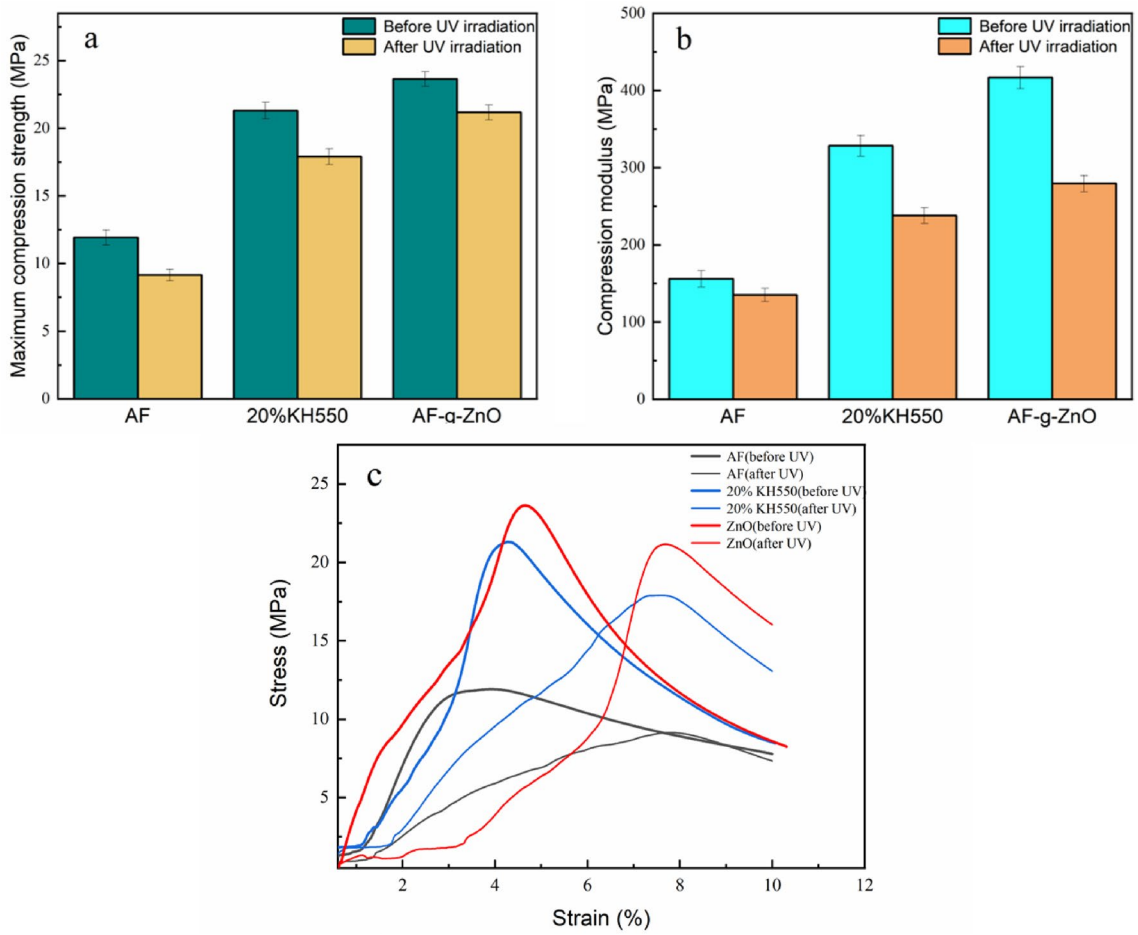

Fig. 25 Comparison of compression tests on aramid composites before and after UV irradiation: **a** maximum compression strength; **b** compression modulus; **c** stress–strain curve

3.8.6 Comparison of the Compression Performance of Samples Not Subjected to and Subjected to UV Exposure

In Fig. 25a and b, the compressive strength retention of the unmodified aramid composites and the 20% KH550-modified composites after UV irradiation was found to be 76.75% and 83.99%, respectively. The aramid composites with ZnO nanowires grown on the surface exhibited a compressive strength of 21.17 MPa after UV irradiation, with a retention rate of 89.56%. This retention rate was 12.8% higher than that of the unmodified composites. It is worth noting that the compressive modulus of all composites was reduced. Comparatively, the retention of flexural and compressive properties in the composites was slightly lower than that of tensile properties. This difference may be attributed to the wider specimens used for flexural and compressive testing, resulting in a larger effective area of UV irradiation. Figure 25c demonstrates that the displacement required to reach the maximum load increases, and the slope of the curve significantly decreases after UV irradiation. This indicates a reduction in the stiffness of the composite. The aramid composites with ZnO nanoparticles grown on the surface exhibited significantly higher retention rates for tensile, flexural, and compressive properties after UV irradiation compared to other modified composites. This observation highlights the considerable impact of this method on improving the UV resistance of aramid composites and enhancing their overall mechanical properties.

4 Conclusion

Numerous measures were employed to enhance the bonding between aramid fibers and epoxy resin, ultimately elevating the mechanical properties and UV resistance of aramid fiber and weft-knitted textile composite materials. In this study, anhydrous calcium chloride and silane coupling agent KH550 were utilized to modify the aramid fiber to enhance its surface activity. Subsequently, a layer of nano-ZnO was

grown on the aramid surface to improve the UV resistance of the fibers. Modified AF impregnated epoxy resin was made into AFRP composites by VARTM molding process. The mechanical properties and interface performance of the aramid composites treated with $CaCl_2$ and KH550 exhibited significant enhancements. The optimal concentration for KH550 modification was determined to be 20%. Mechanical properties and UV resistance of the aramid composites, grafted with ZnO nanoparticles on their surfaces, exhibited remarkable improvement. Tensile, bending, and compressive properties of these composites surpassed those of the 20% KH550-modified counterparts. In addition, an analysis of failure modes in aramid weft-knitted composites under mechanical loading was conducted. Notably, AF-g-ZnO NWs (aramid fiber grafted with ZnO Nanowires) composites displayed remarkable tensile, bending, and compressive strength retention capabilities, reaching 98.08%, 91.49%, and 89.56%, respectively, even after 128 h of UV irradiation. These values significantly outperformed those of unmodified aramid composites, which recorded retention rates of 82.19%, 75.44%, and 76.75%, respectively. The growth of nano-ZnO not only improved the UV resistance of the aramid composites but also led to notable enhancements in the mechanical properties.

Author Contributions CL: provision of study materials and revised the manuscript; JS: writing the initial draft, conducted the trials and analyzing data; YC and MS: assisted JS with trials. CF and LZ: checking the details of the manuscript and helping JS to revise it. All authors commented on previous versions of the manuscript. All authors read and approved the final manuscript.

Funding This work was financially supported by the National Natural Science Foundation of China (Grant nos. 51403154; 11602168).

Data Availability Statement The data supporting the conclusions of this article are available from the corresponding author on reasonable request.

Declarations

Conflict of Interest The author(s) declared no potential conflicts of interest with respect to the research, authorship, and/or publication of this article.

References

1. V.V. Prasad, S. Talupula, A review on reinforcement of basalt and aramid (Kevlar 129) fibers. Mater. Today Proc. **5**(2), 5993–5998 (2018)
2. D. Quan, J.L. Urdaniz, C. Rouge, A. Ivankovic, The enhancement of adhesively-bonded aerospace-grade composite joints using steel fibres. Compos. Struct. **198**, 11–18 (2018)
3. K. Bilisik, G. Erdogan, E. Sapanci, In-plane response of para-aramid/phenolic nanostitched and nanoprepreg 3D composites under tensile loading. Polym. Compos. **40**(4), 1275–1286 (2019)
4. B. Liu, R. Badcock, H. Shu, J. Fang, A superconducting induction motor with a high temperature superconducting armature: electromagnetic theory, design and analysis. Energies **11**(4), 792 (2018)
5. G. Yang, M. Park, S.J. Park, Recent progresses of fabrication and characterization of fibers-reinforced composites: a review. Compos. Commun. **14**, 34–42 (2019)
6. N. Raphael, K. Namratha, B.N. Chandrashekar, K.K. Sadasivuni, D. Ponnamma, A.S. Smitha, S. Krishnaveni, C. Cheng, K. Byrappa, Surface modification and grafting of carbon fibers: a route to better interface. Prog. Cryst. Growth Charact. Mater. **64**(3), 75–101 (2018)
7. W. Lertwassana, T. Parnklang, P. Mora, C. Jubsilp, S. Rimdusit, High performance aramid pulp/carbon fiber reinforced polybenzoxazine composites as friction materials. Compos. B Eng. **177**(9), 107280 (2019)
8. G.C. Qi, B.M. Zhang, S.Y. Du, Y.L. Yu, Estimation of aramid fiber/epoxy interfacial properties by fiber bundle tests and multiscale modeling considering the fiber skin/core structure. Compos. Struct. **167**, 1–10 (2017)
9. H. Sun, H.J. Kong, H.Q. Ding, Q. Xu, J. Zeng, F.Y. Jiang, M.H. Yu, Y.F. Zhang, Improving UV resistance of aramid fibers by simultaneously synthesizing TiO_2 on their surfaces and in the interfaces between fibrils/microfibrils using supercritical carbon dioxide. Polymers **12**(1), (2020). https://doi.org/10.3390/polym12010147
10. M.Z. Li, K. Cheng, C.H. Wang, S.J. Lu, Functionalize aramid fibers with polydopamine to possess UV resistance. J. Inorg. Organomet. Polym. Mater. **31**(7), 2791–2805 (2021)
11. 魏枫, 徐海兵, 颜春, 刘东, 欧阳少波, 裴勇勇, 祝颖丹. 芳香族聚酰胺纤维抗紫外老化的研究进展. 复合材料科学与工程 **0**(6), 115–21 (2022)
12. S. Li, A. Gu, G. Liang, L. Yuan, J. Xue, A facile and green preparation of poly (glycidyl methacrylate) coated aramide fibers. J. Mater. Chem. **122**, 8960–8968 (2012)
13. V. Vilay, M. Mariatti, R. Mat Taib, M. Todo, Effect of fiber surface treatment and fiber loading on the properties of bagasse fiber–reinforced unsaturated polyester composites. Compos. Sci. Technol. **68**, 631–638 (2008)
14. J. Lin, Effect of surface modification by bromination and metalation on Kevlar fibre-epoxy adhesion. Eur. Polym. J. **38**(1), 79–86 (2002)
15. T. Liu, Y. Zheng, J. Hu, Surface modification of aramid fibers with new chemical method for improving interfacial bonding strength with epoxy resin. J. Appl. Polym. Sci. **118**(5), 2541–2552 (2010)
16. G.J. Ehlert, Y. Lin, H.A. Sodano, Carboxyl functionalization of carbon fibers through a grafting reaction that preserves fiber tensile strength. Carbon **49**(13), 4246–4255 (2011)
17. G.S. Sheu, S.S. Shyu, Surface properties and interfacial adhesion studies of aramid fibres modified by gas plasmas. Compos. Sci. Technol. **52**(4), 489–497 (1994)
18. Y. Zhang, Z. Jiang, Y. Huang, Q. Li, The modification of Kevlar fibers in coupling agents by γ-ray co-irradiation. Fibers Polym. **12**(8), 1014–1020 (2011)
19. M. Andideh, M. Esfandeh, Effect of surface modification of electrochemically oxidized carbon fibers by grafting hydroxyl and amine functionalized hyperbranched polyurethanes on interlaminar shear strength of epoxy composites. Carbon **123**, 233–242 (2017)
20. L.W. Zhang, H.J. Kong, M.M. Qiao, X.M. Ding, M.H. Yu, Supercritical CO_2-induced nondestructive coordination between ZnO nanoparticles and aramid fiber with highly improved interfacial-adhesion properties and UV resistance. Appl. Surf. Sci. **521**, (2020). https://doi.org/10.1016/j.apsusc.2020.146430
21. C.Y. Li, J.J. Song, W.J. Xing, L.X. Wang, Y.Y. Cui, X.Y. Pei, Mechanical properties of interlayer hybrid textile composite materials based on modified aramid and UHMWPE fabrics. Polym. Adv. Technol. **34**(1), 205–216 (2023)

22. L.X. Ma, J.W. Zhang, C.Q. Teng, Covalent functionalization of aramid fibers with zinc oxide nano-interphase for improved UV resistance and interfacial strength in composites. Compos. Sci. Technol. **188**, (2020). https://doi.org/10.1016/j.apsusc.2020.146430
23. 管宇, 冒亚红. 八聚(γ-氨丙基)倍半硅氧烷对芳纶纤维的抗紫外接枝改性. 纺织科学与工程学报 **35**(01), 46–55 (2018)
24. A. Xie, Z. Zhang, B. Gu, G. Yang, D. Tao, S. Weng, J. Mater. Sci. Lett. **21**, 345 (2002)
25. Z. Jin, Z. Luo, S. Yang, S. Lu, J. Appl. Polym. Sci. **132**, n/a (2015)
26. R. Sa, Y. Yan, Z. Wei, L. Zhang, W. Wang, M. Tian, A.C.S. Appl, Mater. Interfaces **6**, 21730 (2014)
27. H. Awais, Y. Nawab, A. Anjang et al., Effect of fabric architecture on the shear and impact properties of natural fibre reinforced composites. Compos. Part B Eng. **195**, (2020). https://doi.org/10.1016/j.compositesb.2020.108069
28. S.D. Pandita, D. Falconet, I. Verpoest, Impact properties of weft knitted fabric reinforced composites. Compos. Sci. Technol. **62**(7–8), 1113–1123 (2002)
29. J. Tian, L.Z. An, Y.F. Tan, T. Xu, X.T. Li, G.X. Chen, Graphene oxide-modified aramid fibers for reinforcing epoxy resin matrixes. ACS Appl. Nano Mater. **4**(9), 9595–9605 (2021)
30. 向坤, 李扬, 陆轴, 周筑文, 熊德永, 罗筑. 低温等离子体处理芳纶复合材料界面性能研究进展. 工程塑料应用 **48**(06), 145–149 (2020)
31. GB/T 19975–2005, 高强化纤长丝拉伸性能试验方法[s]
32. C.Y. Li, Y.Y. Cui, W.J. Xing, X.Y. Pei, J.J. Song, L.X. Wang, Secondary silane grafting on aramid fibers improves the interfacial bonding performance in textile composite materials. J. Compos. Mater. **56**(29), 4421–4432 (2022)
33. GB/T 1447-2005, 纤维增强塑料拉伸性能试验方法[S]
34. GB/T 1449-2005, 纤维增强塑料弯曲性能试验方法[S]
35. GB/T 1448-2005, 纤维增强塑料压缩性能试验方法[S]
36. A. Nejman, I. Kaminska, I. Jasinska, G. Celichowski, M. Cieslak, Influence of low-pressure RF plasma treatment on aramid yarns properties. Molecules **25**(15), (2020). https://doi.org/10.3390/molecules25153476
37. R.N. Sa, Y. Yan, Z.H. Wei, L.Q. Zhang, W.C. Wang, M. Tian, Surface modification of aramid fibers by bio-inspired poly(dopamine) and epoxy functionalized silane grafting. ACS Appl. Mater. Interfaces **6**(23), 21730–21738 (2014)
38. C.T. Li, N. Wu, M. Zhang, C.H. Wei, F. Yan, Z.H. Wang, Effects of E44 and KH560 modifiers on properties of distillers grains poly(butylene succinate) composites. Polym. Compos. **40**(4), 1499–1509 (2019)
39. R. Yang, Y. Li, J. Yu, Photo-stabilization of linear low density polyethylene by inorganic nano-particles. Polym. Degrad. Stab. **88**(2), 168–174 (2005)
40. H.X. Zhao, R.K.Y. Li, A study on the photo-degradation of zinc oxide (ZnO) filled polypropylene nanocomposites. Polymer **47**(9), 3207–3217 (2006)
41. Z.W. Xu, L. Chen, Y.D. Huang, J.L. Li, X.Q. Wu, X.M. Li, Y.N. Jiao, Wettability of carbon fibers modified by acrylic acid and interface properties of carbon fiber/epoxy. Eur. Polym. J. **44**(2), 494–503 (2008)